Nanoscale

PAPER

View Article Online
View Journal | View Issue

Cite this: *Nanoscale*, 2017, **9**, 13104

1D copper nanowires for flexible printable electronics and high ampacity wires†

Atif Aziz, *‡[a] Tan Zhang, ‡[b] Yen-Hao Lin,[b] Farhad Daneshvar,[b] Hung-Jue Sue*[b] and Mark Edward Welland[a]

Received 7th April 2017,
Accepted 9th August 2017

DOI: 10.1039/c7nr02478a

rsc.li/nanoscale

This paper addresses the synthesis and a detailed electrical analysis of individual copper nanowires (CuNWs). One dimensional CuNWs are chemically grown using bromide ions (Br^-) as a co-capping agent. By partially replacing alkyl amines with Br^-, the isotropic growth on Cu seeds was suppressed during the synthesis. To study the electrical properties of individual CuNWs, a fabrication method is developed which does not require any e-beam lithography process. Chemically grown CuNWs have an ampacity of about 30 million amps per cm^2, which is more than one order of magnitude larger than bulk Cu. These good quality, easy to synthesize CuNWs are excellent candidates for creating high ampacity wires and flexible printable electronics.

Introduction

One dimensional (1D) conducting wires are important building blocks of nanotechnology devices. Preparation of 1D nanowires can broadly be divided into two types. The first type needs a substrate or a template to be grown or supported. For example, growth of nanowires or carbon nanotubes on a substrate,[1,2] growth of nanowires using alumina templates[3] or the fabrication of nanowires using any lithography process comes into this category. The second type is the one where nanowires can be grown without a substrate or a template. For example, nanowires grown in a chemical using a hydrothermal process.[4] The chemical growth of nanowires is particularly useful for creating cost effective nanowires in a large quantity. The main advantage is that the chemical growth methods can be scaled up to an industrial level.

Due to recent developments in flexible, stretchable and wearable electronics, and display technology, highly conductive printable transparent conductors are highly desirable. Low dimensional conducting materials are particularly suitable for integrating with flexible substrates. If the electrical conductivity of the nanowires is high, a low density network of nanowires can be used as a transparent conductor. For example, Ag nanowires have been used for creating flexible, transparent and stretchable electrodes.[5–7] Cu,[4] Au[8] and Ag[9] are some of the conducting metals which can be chemically grown into long nanowires without any substrate or template. In particular, Cu has one of the highest electrical conductivities ($\sim 6 \times 10^5$ S cm^{-1}) among materials. It is also much cheaper than Ag and Au, and abundant in nature. Therefore, Cu is a material of choice for applications which require high electrical conductivity and flexibility. Copper nanowires (CuNWs) also have a high electrical conductivity compared to metal oxides like ITO (indium tin oxide)[10] or carbon based materials.[11] In this paper we study the chemical growth of low dimensional Cu nanostructures using a hydrothermal process and a co-capping agent, and investigate the electrical properties and the failure mechanisms of the individual nanowires.

CuNWs can be chemically grown to hundreds of microns in length. These nanowires can make a network of highly flexible conducting wires. One drawback is that the CuNW surface can get oxidized in air; either a capping layer like polyimide or PDMS can be used to protect it from oxidation or CuNWs can be covered with a graphene layer.[12] For large area applications, methods like photonic welding or laser induced photothermochemical reduction of Cu_xO NWs to CuNWs can also be used for improving conductive links between CuNWs.[13,14] Electrical properties of CuNWs are commonly measured using sheet resistance,[15] where the current passes through a percolation path. It provides some electrical conductivity information which is averaged over a large but unknown number of nanowires. High contact resistance, which is due to a large number of wire junctions, dominates the resistance and therefore it is difficult to measure the true electrical conductivity and the ampacity of the CuNWs. To understand the quality of nano-

[a]*Nanoscience Centre, Department of Engineering, University of Cambridge, CB3 0FF, UK. E-mail: aa267@cam.ac.uk*
[b]*Polymer Technology Centre, Department of Materials Science and Engineering, Texas A&M University, College Station, TX 77843, USA. E-mail: hjsue@tamu.edu*

†Electronic supplementary information (ESI) available: Additional SEM images of Cu nanocrystals, contact resistance and Pt conductivity. See DOI: 10.1039/c7nr02478a

‡These authors contributed equally.

wires, individual CuNWs must be analyzed. Xu *et al.* studied the transport properties of a single Cu nanowire but they could not determine the ampacity of the CuNWs because their Pt contacts had lower ampacity than CuNWs.[16] In this work, we have developed a simple method, which does not require an e-beam lithography process, to fabricate transport devices using a single CuNW and these devices do not suffer from the problem faced by Xu *et al.* Electrical properties, which include electrical conductivity, current carrying capacity, and failure mechanism, of the chemically synthesized CuNWs were carefully investigated.

Synthesis of Cu nanowires (CuNWs)

Synthesis of CuNWs by a hydrothermal method has been considered as a promising strategy for large-scale production of nanomaterials.[17] In a typical synthesis system, as illustrated in Fig. 1(a), copper ions, Cu(I) or Cu(II), are reduced to Cu(0) seeds, and then 1D growth on these nanocrystal seeds in aqueous or organic solutions leads to the formation of CuNWs.[18–20] Among these systems, alkyl amines are mostly used, because they not only serve as a capping agent but can also form complexes with other reactants to promote seed formation and the chemical reduction process.[21,22] This multifunctional role makes alkyl amines irreplaceable in Cu nanowire synthesis. However, it is a challenge to use alkyl amines as a sole capping agent to produce clean CuNWs because a relatively large fraction of other shapes for Cu nanocrystals, such as particles, cubes, is also produced, as seen in Fig. 2.

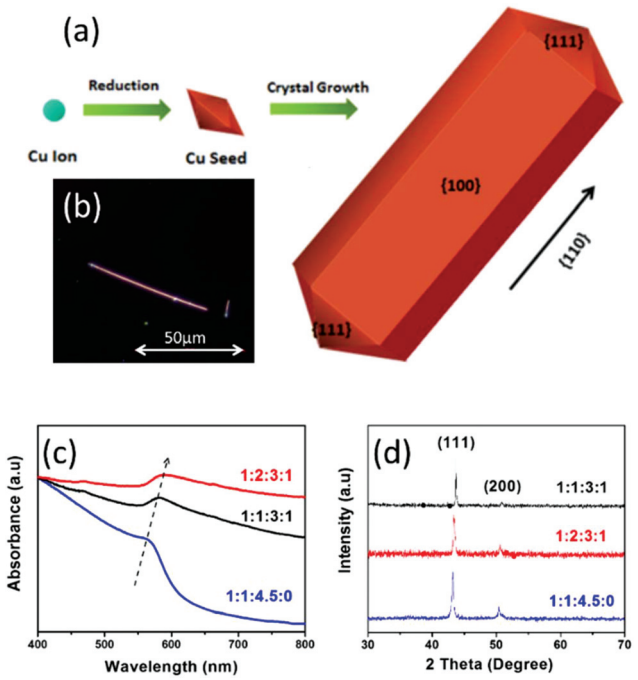

Fig. 1 (a) Schematic representation of Cu nanowire synthesis using a hydrothermal method. (b) Dark field optical image. (c) UV-Vis spectra and (d) XRD patterns of the as-synthesized 1D CuNWs.

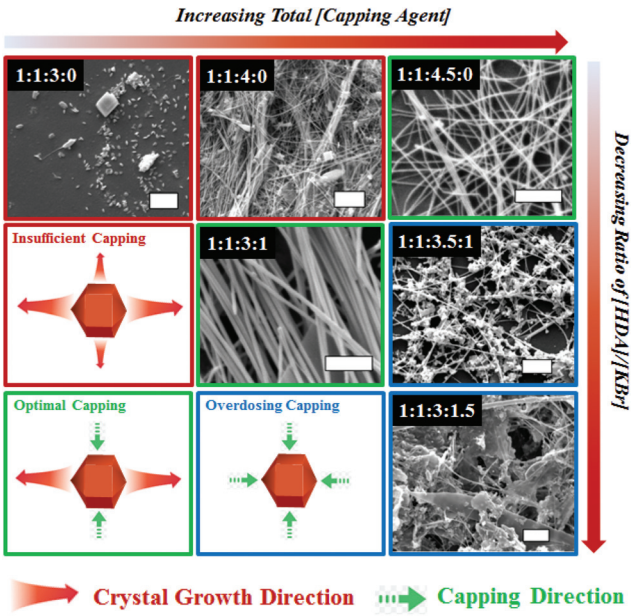

Fig. 2 Schematic demonstration of the capping effect on the growth of Cu nanocrystals, and the scanning electron micrographs of the Cu nanocrystals synthesized with different molar ratios of $CuCl_2$: glucose : HDA : KBr. Scale bars = 2 μm.

The capping insufficiency is the reason for the isotropic crystal growth in these systems.

In order to better control the growth kinetics to suppress the isotropic crystal growth, one solution is to incorporate a co-capping agent to modify the capping efficiency. Bromide ions (Br^-) have been widely used to initiate the anisotropic growth on Au, Ag or Pt nanocrystals.[23] Similar to alkyl amines, Br^- preferentially adsorbs onto the {100} facet on metal nanocrystals to restrict the growth direction.[23] The ionic species with a relatively small size like Br^- can have a better capping effect than alkyl amines on Cu seeds. In this work, we introduced Br^- as a co-capping agent to produce good quality CuNWs.

A precursor solution was obtained by dissolving copper chloride ($CuCl_2$), glucose, hexadecylamine (HDA) and potassium bromide (KBr) in 60 mL deionized water. A uniform blue color solution was formed after stirring, indicating the formation of Cu(II)–HDA complexes.[22] The precursor solution was then maintained at 110 °C for 16 h without stirring, and the color of the solution changed from blue to pink and then to reddish brown. The color change in the solution indicated that the Cu(II)–HDA complexes have been reduced to Cu seeds, likely through Maillard's reaction,[21] and then formed CuNWs *via* a 1D nanocrystal growth.

The molar ratio of Cu and capping agent is critical for the control of nanocrystal growth. In the absence of Br^-, the capping on Cu nanocrystals was carried out using HDA alone. The preferential adsorption of HDA on the {100} facets could suppress the crystal growth on these facets to initiate an anisotropic growth.[18] However, as seen in Fig. 2, the sample with a molar ratio of 1 : 1 : 3 : 0 ($CuCl_2$: glucose : HDA : KBr, herein-

after), only produced Cu nanoparticles and nanocubes, indicating an isotropic growth dominated system. The reason is because the concentration of HDA was insufficient to cover all newly formed {100} facets on Cu nanocrystals in this sample. These exposed facets are active for Cu crystal growth, which was demonstrated as insufficient capping in Fig. 2. With an increased concentration of HDA, CuNWs started to form in the system, indicating that anisotropic growth started to dominate the systems. With a molar ratio of 1 : 1 : 4.5 : 0, a large fraction of CuNWs with a diameter of 72 ± 13 nm were obtained.

Incorporation of Br^- could modify the capping efficiency of Cu nanocrystals. For example, the nanoparticle formation can be suppressed using Br^- as a co-capping agent to partially replace HDA. As shown in Fig. 2, approximately 60% of CuNWs and 40% of nanoparticles were obtained using a molar ratio of 1 : 1 : 4 : 0. With the same molar ratio of Cu and total capping agent, clean CuNWs with only a trace amount (about 2–3%) of nanoparticles were synthesized by replacing one quarter of HDA with Br^-, *i.e.*, using a molar ratio of 1 : 1 : 3 : 1. It is well known that nanowires grow from multi-twinned seeds.[24] However, multi-twinned seeds are unstable at initial stages if their {100} facets are not well capped. The crystal growth on the {100} facets could rapidly develop multi-twinned seeds into single-crystal seeds,[25] which only produce nanoparticles. Compared with more hydrophobic HDA molecules, Br^- is a small ionic component which can diffuse faster in an aqueous environment, and easier to be chemisorbed onto nanocrystals, especially onto small nanocrystals (<10 nm).[25] Br^- was also found to facilitate the maturing process for Cu nanocrystals growing in a non-aqueous environment.[26] These features of Br^- ensure a complete capping on multi-twinned seeds, which is critical to suppress isotropic growth.

The ratio of the HDA and KBr is also important because different HDA : KBr ratios result in different capping efficiencies on Cu nanocrystals. On the one hand, insufficient Br^- cannot provide enough capping protection on Cu seeds, resulting in insufficient capping. On the other hand, overdosing Br^- can also reduce Cu nanowire formation. If the {100} facets on Cu nanocrystals have been saturated by the capping agent, extra Br^- can also cap the {110} and {111} facets on Cu nanocrystals.[19] As demonstrated in Fig. 2, overdosing capping can suppress the overall growth of Cu seeds, resulting in the formation of small Cu nanocrystals. Sometimes, these small nanocrystals may aggregate to form plate-like structures.[25] This is the reason why using Br^- alone cannot produce CuNWs.[19] In this study, an optimal molar ratio to produce CuNWs was found to be 1 : 1 : 3 : 1 ($CuCl_2$: glucose : HDA : KBr). The samples with a lower or higher HDA : KBr ratio produced more small nanoparticles. Additional SEM images can be found in the ESI.†

The CuNW formation is also affected by the chemical reduction process. The rate of reduction is usually adjustable by varying the concentration of the reducing agent, or glucose in this study. More glucose in the system can increase the rate of chemical reduction. In this scenario, faster growth on Cu seeds could lead to more seeds developed from multi-twinned to single-crystal if capping agent failed to stop the crystal growth on the {100} facets in time. Fig. 3 shows the effect of glucose concentration on CuNW formation. As expected, more small nanoparticles were observed when the concentration of glucose was doubled in the absence of Br^- (1 : 2 : 4.5 : 0). Interestingly, a similar phenomenon was not observed for the samples with Br^-. The nanoparticle formation was still suppressed even though we doubled the concentration of glucose, *i.e.*, using a molar ratio of 1 : 2 : 3 : 1. It was confirmed that using Br^- as a co-capping agent can protect the {100} facets on Cu seeds efficiently. As a result, the isotropic growth on Cu nanocrystals was suppressed in the presence of Br^-.

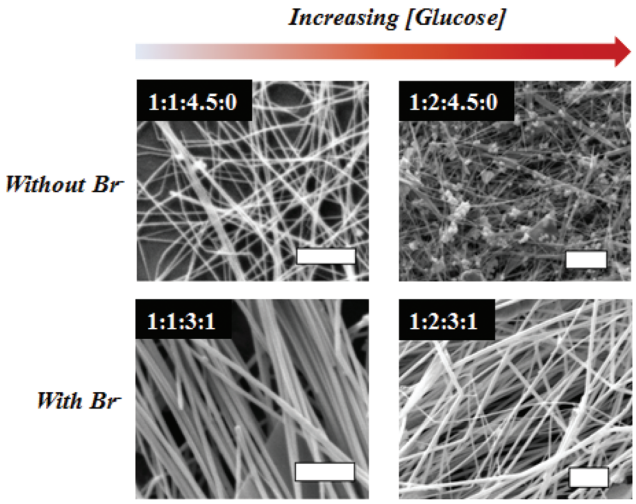

Fig. 3 Scanning electron micrographs of the Cu nanowires synthesized with different molar ratios of $CuCl_2$: glucose : HDA : KBr. Scale bars = 2 μm.

The diameter of CuNWs synthesized using Br^- was found to be 176 ± 29 nm which is larger than that without using Br^- (72 ± 13 nm). This observation was confirmed using UV-Vis spectroscopy (Fig. 1(c)). Compared with the Br^- free sample (1 : 1 : 4.5 : 0), the maximum absorption peaks for the CuNWs synthesized using Br^- shifted to higher wavenumbers. Because of the surface plasmon resonance effect,[22] this redshift suggests that the CuNWs in these samples (1 : 1 : 3 : 1 and 1 : 2 : 3 : 1) have a larger average nanowire diameter. One possible reason for the increase in nanowire diameter is that although Br^- could protect the Cu seeds in the early stages, the competitive adsorption between Br^- and HDA might reduce the packing density for the HDA layers on the {100} facets, resulting in CuNWs with a larger diameter.[26] The other possibility is due to the aforementioned multi-functional role of HDA. HDA is also involved in other processes, such as seeding, complexation and reduction. Br^-, as far as we know, does not participate in these processes. In addition to the capping effect, partially replacing HDA with Br^-, therefore, might contribute to other effects on the dislocation-driven growth of Cu seeds, and consequently produces CuNWs with different diameters.[27] The XRD patterns of the as-synthesized

CuNWs (Fig. 1(d)) are consistent with face-centered-cubic Cu without a significant amount of other impurities. The CuNWs synthesized using a molar ratio of 1 : 1 : 3 : 1 were selected for electrical measurement.

Fabrication of CuNW transport devices

CuNW transport devices were fabricated using an aligned landing of nanowires onto the titanium/gold (Ti/Au) electrodes. The main advantage of this technique is that no complex e-beam lithography is required. The schematic of the process is shown in Fig. 4(a). First, Ti/Au contacts were fabricated using photolithography and a lift off process on a Si/SiO_2 (60 nm) wafer. A 10 nm Ti layer and then 200 nm Au layer were deposited using an e-beam evaporator. A small drop of ethanol solution which contains CuNWs was placed, using a pipette, on a thin (~200 μm) polydimethylsiloxane (PDMS) film and left to dry. CuNWs were 200 nm in diameter and about 50 μm long. These wires could be seen using an optical microscope. PDMS was then attached to the glass slide. An MBJ4 mask aligner was used to align an isolated CuNW on the PDMS layer with the Au electrodes. Immediately before performing the alignment process, a silicon chip which had Ti/Au electrodes was cleaned with oxygen plasma with a RF (Radio Frequency) power of 100 W and a pressure of 0.4 mbar for five minutes. Once aligned, the silicon chip was slowly raised until it was in contact with the PDMS. The sample was then left to remain in contact for two minutes. PDMS was then slowly removed by lowering the Si wafer down. The transfer was performed using the medium retention 6.5 mil PF-40-X4 film from Gel-Pak and no heating was required to transfer the CuNWs. Fig. 4(b) and (c) show the SEM images of the CuNWs after being transferred on the Ti/Au electrodes and Fig. 4(d) is the dark field optical image of the CuNWs on the Ti/Au electrodes.

Electrical measurements

Four terminal electrical measurements were performed using a Keithley 5200 SCS parameter analyzer. The device geometry is shown in Fig. 5(d). The current was applied between the electrodes I1 and I2 and the voltage drop across the CuNW was measured using the voltage leads V1 and V2. When CuNWs are exposed to air, a thin oxide layer on the Cu wires prevents electrical contact between the nanowire and the Au electrodes. To establish the lowest possible contact resistance, a few nanometers of the CuNW was etched using gallium focused ion beam (Ga-FIB) milling and then about 200 nm thick, 1 μm wide and 5 μm long platinum (Pt) pads were deposited using a Ga-FIB, as shown in Fig. 5(c).

The Pt contact resistance is measured by drawing the resistance of CuNW1, CuNW2 and CuNW3 as a function of their length, as shown in Fig. S2.† The contact resistance is about 9 Ω. Table 1 shows the electrical conductivity and the maximum current density or ampacity of 1D CuNWs measured at room temperature. The electrical conductivity of the nanowires is a little less than Cu. However, the maximum current density of all the CuNWs is close to 3×10^7 A cm^{-2}, which is more than an order of magnitude larger than the bulk Cu wires.

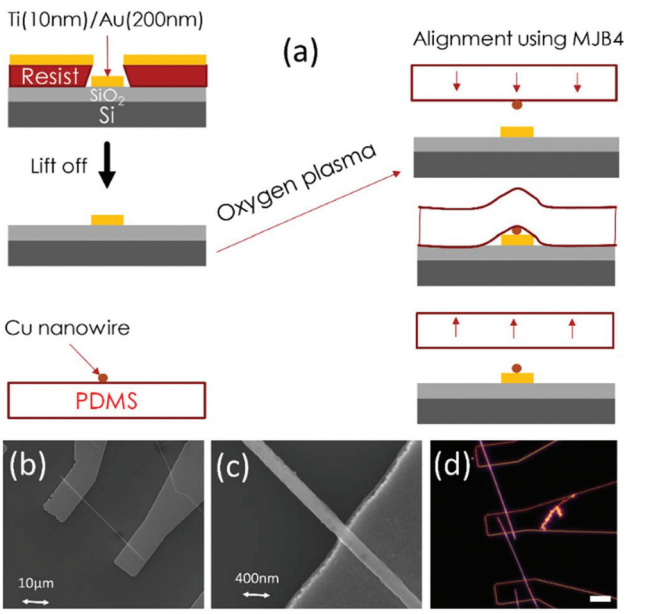

Fig. 4 (a) Schematic of the CuNW transfer process from PDMS to the Ti/Au electrode on a Si/SiO_2 wafer. (b, c) SEM images of the CuNW after landing on the Ti/Au electrodes. (d) Dark field optical image of the CuNWs after being transferred on the Ti/Au electrodes. Scale bar = 10 μm.

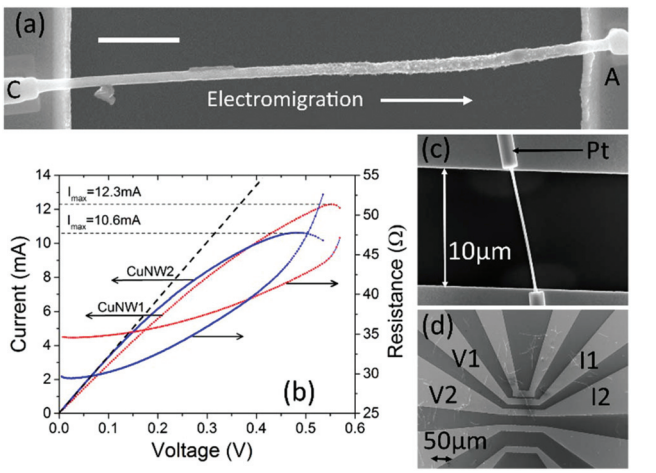

Fig. 5 (a) SEM of a CuNW after a large current passes through the wire. Scale bar is 2 μm. The anode and cathode are labelled A and C respectively. It shows the effect of electromigration. Electromigration is in the direction of the anode electrode. The length of the wire is about 14 μm. (b) *I*–*V* curves and the corresponding resistance of the nanowires CuNW1 and CuNW2. I_{max} is the maximum current that passes through the CuNW, after which the current reduces and the nanowire becomes an open circuit. The dashed line is a straight line drawn along the linear region of the *I*–*V* curve. (c) SEM image of the device after Pt deposition using a Ga focused ion beam. (d) SEM image of the four-probe device geometry.

Table 1 Dimensions, conductivity and the maximum current density of the 1D CuNW

Sample	Length L, (μm)	Diameter d, (nm)	Electrical conductivity, σ (S cm^{-1})	Max. current density, J_{max} (A cm^{-2})
Cu(bulk)			5.9×10^5	1.0×10^6
CuNW1	28.5	200	3.5×10^5	3.9×10^7
CuNW2	20	190	3.4×10^5	3.7×10^7
CuNW3	11	190	3.4×10^5	3.9×10^7

The I–V curves and the resistance of the samples CuNW1 and CuNW2 are plotted in Fig. 5(b). The I–V curves are linear up to about 2 mA. Nanowires show a linear (ohmic) behaviour at low bias, as indicated by the projected dashed line. However, as the current is increased further, the resistance of the wire is noticeably increased due to the Joule heating and the I–V curve becomes non-linear. After the current reaches the maximum value at I_{max}, the current drops and CuNW becomes an open circuit. The ampacity of the CuNW is defined as the maximum current density which flows through the wire before it becomes an open circuit. On average, the ampacity of these high aspect ratio CuNWs is $J = 3.8 \times 10^7$ A cm^{-2}, which shows that the chemically grown CuNWs are of good quality and exhibit low density of defects.

Discussion and analysis

The electrical conductivity of the CuNWs is extracted from the linear regime of the I–V curve, and after subtracting the 9 Ω Pt contact resistance, the electrical conductivity of the CuNWs is calculated to be 3.4×10^5 S cm^{-1}. It is lower than the electrical conductivity of the bulk Cu, which is typically 5.95×10^5 S cm^{-1}. Since the width of the wire is greater than the electron mean free path in Cu, which is about 40 nm,[28] the grain boundaries rather than surface scattering is the dominant mechanism for this lower electrical conductivity. Similar conductivity values (1.8×10^5 S cm^{-1} and 2.8×10^5 S cm^{-1}) have been reported for e-beam evaporated and other hydrothermal CuNWs, respectively.[16,29] As compared to chemically grown nanowires, Cu nanowires created using pulsed electrodeposition have a lower ampacity of about 2×10^6 A cm^{-2} whereas CuNWs grown in a vacuum using e-beam evaporation have a higher ampacity of about 1×10^8 A cm^{-2}. It should be noted that these CuNWs have a much smaller aspect ratio than the ones studied here.[30,31]

At high current density, the nanowire experiences a thermal as well as an electromigration stress. The CuNW is connected to the Au electrodes, which function as heat sinks, on both ends. The temperature profile along the nanowire and the heat sink is calculated using the heat transfer equation $\nabla^2 T - m^2 T + Q/k = 0$,[32] where $m = \sqrt{k_{sub}/ktd}$ and $Q = J^2\rho$. The wire is considered as a rectangular wire of width and thickness t = 200 nm and a length of $2L$ = 28 μm. The values used for the thermal conductivities of the wire and the substrate are k = 385 W K^{-1} m^{-1} and k_{sub} = 0.55 W K^{-1} m^{-1}, respectively. The thickness of the oxide layer underneath the CuNWs is d = 60 nm, and the current density at which the temperature profile is calculated is $J = 3.9 \times 10^7$ A cm^{-2}. The temperature profile of the CuNWs is shown in Fig. 6(a). It shows that the temperature is maximum (approximately 140 °C) at the centre of the wire, and the temperature gradient is the highest near the edges. It also shows that the heat is mainly dissipating from the contact pads. Similar distribution was also observed in silver nanowires.[33] The temperature increase causes the wire to expand with respect to the substrate and therefore creates a thermal stress. Thermal stress is proportional to the thermal coefficient of expansion (β), Young's modulus (B) and a change in temperature (ΔT) of the nanowire. Fig. 6(b) shows the thermal stress along the wires, calculated using the equation: Thermal stress = $-3\beta B\Delta T$, where 3 comes from the geometrical factor and negative sign represents the compressive stress, the thermal expansion coefficient of Cu relative to SiO_2 used for this calculation is $\beta = 17 \times 10^{-6}$ °C^{-1} and Young's modulus is B = 120 GPa.

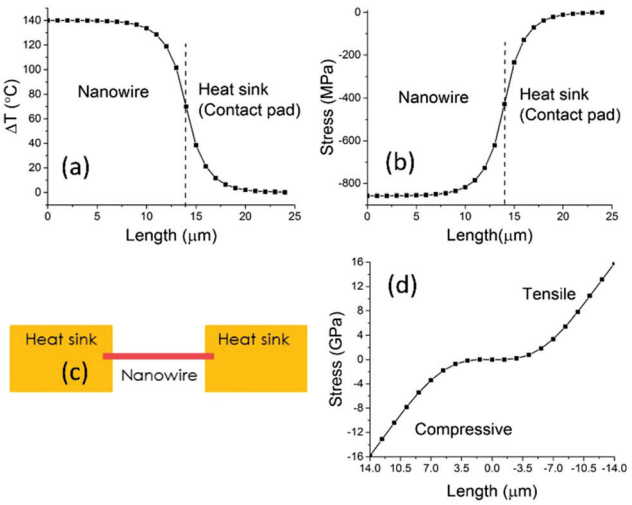

Fig. 6 (a) The calculated temperature difference profile of the CuNW at 12.3 mA. (b) Thermal stress experienced by the CuNW as a function of length. (a) and (b) shows the profiles from the center of the wire to the heat sink. Due to symmetry, the profile should be the same for the other half of the wire. (c) The cartoon of the device. (d) Compressive and tensile stress experienced by the CuNW due to electromigration.

At high current density, the electron wind transfers enough momentum to the Cu atoms such that they are displaced in the direction of the electron flow, leaving behind vacancies. Accumulation of vacancies causes tensile stress; whereas, an accumulation of Cu results in compressive stress. Since vacancies are accumulated near the cathode, tensile stress occurs at the cathode end of the wire; whereas, compressive stress builds up near the anode. Fig. 5(a) shows the CuNW after a current density of 1×10^7 A cm^{-2} passes through the CuNW. To observe the Cu mass transfer due to an electromigration (EM) effect, voltage was swept at the rate of 0.4 mV s^{-1}.

This image shows that the Cu atoms are accumulated near the anode end of the transport device. The EM stress of the CuNW1 sample at 12.3 mA current is calculated using the equation below and is plotted in Fig. 6(d):[34]

$$\sigma = 2GL\left(-\frac{x}{2L} - 4\sum_{n=0}^{\infty}\left(\frac{1}{\eta^2}e^{-\eta t/\tau}\cos\left(\eta\frac{x+L}{2L}\right)\right)\right)$$

where $G = Eq/\Omega$ is the EM driving force, $\eta = (2n + 1)\pi$ and $\tau = 4L^2/\kappa$; $\kappa = DB\Omega/k_BT$ and $E = J\rho$. D, B, Ω and q are the effective atomic diffusivity, Young's modulus, atomic volume and the effective atomic charge respectively. J is the current density and ρ is the resistivity of the Cu wire.

By comparing between Fig. 6(b) and (d), stress caused by the electromigration is much greater than that due to the thermal stress. The failure location of the wire also gives a good indication of the mechanism involved in breaking the nanowire at a high current density. If the failure occurs at the centre of the wire, Joule heating is generally the dominant failure mechanism, as observed by Yeo *et al.* in silver nanowires.[33] Whereas, if failure occurs at the electrode ends of the wire, tensile or compressive stress due to electromigration causes the wire to fail. We have observed that the CuNWs always fail near the cathode end of the wire, which also shows that tensile stress due to electromigration is the dominant failure mechanism for these CuNWs. Therefore, the ampacity of the CuNW is limited by the electron migration process. The high ampacity in these nanowires, as compared to bulk Cu, is most likely due to the delayed onset of electromigration since the presence of voids between metal grains helps the onset of the electromigration process. High ampacity indicates that the grains in chemically grown Cu nanowires are well packed and free of voids.

Conclusion

In summary, Br^- has been used as a co-capping agent to partially replace alkyl amines to synthesize CuNWs. During the reaction, multi-twinned Cu seeds were efficiently protected by Br^-, especially at their initial stages, to suppress isotropic growth. With an optimal capping agent ratio of 3 : 1 (HDA : Br^-), clean CuNWs with good electrical conductivity and ampacity were synthesized. These CuNWs can be used in various applications that demand high thermal and electrical conductivity and ampacity. Since CuNWs can sustain a high current density, due to their good ampacity, only a very low number of chemically grown CuNWs are needed for making transparent and flexible conductors. The CuNWs possess an ampacity one order of magnitude higher than bulk Cu, and found to be limited by the electron migration process. If electromigration can be suppressed further, the ampacity of the CuNW can be increased further. Despite the fact that these CuNWs are grown using a simple solution method, which does not require any vacuum processing, they have a high ampacity and good conductivity. These high quality CuNWs can lead to more reliable and robust devices. It is anticipated that high ampacity material systems containing CuNWs can be produced for many important industrial applications, including microelectronic devices, electrical vehicles, flexible, stretchable and transparent devices, composite materials and power grids for energy transmission.

Experimental section

Materials used

Copper chloride ($CuCl_2$, from Alfa Aesar), glucose (from TCI), hexadecylamine (HDA, from Merck) and potassium bromide (KBr, from J.T. Baker) were used as received.

Cu nanowire (CuNW) synthesis

In the precursor solution, typically 0.75 mmol $CuCl_2$, 0.75 mmol glucose, and different moles of hexadecylamine (HDA) and KBr were dissolved in 60 mL deionized water. The mixtures were stirred for 7 h, and then maintained at 110 °C for 16 h without stirring. The products were collected by centrifugation at 6000 rpm for 10 min, and washed with deionized water, hexane and ethanol 2–3 times each until the supernatant turned clear. The products were stored in ethanol.

Characterization

The structural properties and the morphologies of the as-synthesized CuNWs were examined using an ultraviolet-visible near-infrared spectrophotometer (Shimadzu UV-3600), an X-ray powder diffractometer (Bruker D8 focus Bragg Brentano) and a scanning electron microscope (FEI Quanta 600 FE-SEM).

Fabrication of devices

To optimize the transfer of CuNWs onto the gold electrodes different types of PDMS films (PF-30-XT, PF-40-X4, PF-10/17-X4 and PF-60-X8) from Gel-Pak were tested. The best transfer was obtained by using the medium retention 6.5 mil PF-40-X4 film. Platinum pads were deposited using the FEI FIB200 system at 30 keV and 13 pA. It took about 3 min to deposit 200 nm thick Pt of dimensions 5 μm × 1 μm, with a dwell time of 0.2 μs. The electrical conductivity of the FIB deposited Pt was 4.7×10^2 S cm^{-1}, see Fig. S3.†

Conflicts of interest

There are no conflicts to declare.

Acknowledgements

The authors acknowledge the support from the Lloyd's Register Foundation, London, UK, who funded this research through grants to protect life and property by supporting engineering-related education, public engagement and the application of research.

Notes and references

1 J. Robertson, Growth of Nanotubes for Electronics, *Mater. Today*, 2007, **10**, 36–43.

2 W. I. Park, D. H. Kim, S. W. Jung and G. C. Yi, Metalorganic Vapor-Phase Epitaxial Growth of Vertically Well-Aligned ZnO Nanorods, *Appl. Phys. Lett.*, 2002, **80**, 4232–4234.

3 X. Xu, X. Fang, H. Zeng, T. Zhai, Y. Bando and D. Golberg, One-Dimensional Nanostructures in Porous Anodic Alumina Membranes, *Sci. Adv. Mater.*, 2010, **2**, 273–294.

4 S. Ye, I. E. Stewart, Z. Chen, B. Li, A. R. Rathmell and B. J. Wiley, How Copper Nanowires Grow and How to Control Their Properties, *Acc. Chem. Res.*, 2016, **49**, 442–451.

5 S. Hong, H. Lee, J. Lee, J. Kwon, S. Han, Y. D. Suh, H. Cho, J. Shin, J. Yeo and S. H. Ko, Highly Stretchable and Transparent Metal Nanowire Heater for Wearable Electronics Applications, *Adv. Mater.*, 2015, **27**, 4744–4751.

6 J. Lee, K. An, P. Won, Y. Ka, H. Hwang, H. Moon, Y. Kwon, S. Hong, C. Kim, C. Lee, *et al.*, A Dual-Scale Metal Nanowire Network Transparent Conductor for Highly Efficient and Flexible Organic Light Emitting Diodes, *Nanoscale*, 2017, **9**, 1978–1985.

7 B. Bari, J. Lee, T. Jang, P. Won, S. H. Ko, K. Alamgir, M. Arshad and L. J. Guo, Simple Hydrothermal Synthesis of Very-Long and Thin Silver Nanowires and Their Application in High Quality Transparent Electrodes, *J. Mater. Chem. A*, 2016, **4**, 11365–11371.

8 F. Kim, K. Sohn, J. S. Wu and J. X. Huang, Chemical Synthesis of Gold Nanowires in Acidic Solutions, *J. Am. Chem. Soc.*, 2008, **130**, 14442–14443.

9 L. F. Gou, M. Chipara and J. M. Zaleski, Convenient, Rapid Synthesis of Ag Nanowires, *Chem. Mater.*, 2007, **19**, 1755–1760.

10 T. Minami, Transparent Conducting Oxide Semiconductors for Transparent Electrodes, *Semicond. Sci. Technol.*, 2005, **20**, S35–S44.

11 D. J. Lipomi, M. Vosgueritchian, B. C.-K. Tee, S. L. Hellstrom, J. a. Lee, C. H. Fox and Z. Bao, Skin-like Pressure and Strain Sensors Based on Transparent Elastic Films of Carbon Nanotubes, *Nat. Nanotechnol.*, 2011, **6**, 788–792.

12 Y. Ahn, Y. Jeong, D. Lee and Y. Lee, Copper Nanowire-Graphene Core-Shell Nanostructure for Highly Stable Transparent Conducting Electrodes, *ACS Nano*, 2015, **9**, 3125–3133.

13 K. Mallikarjuna, H.-J. Hwang, W.-H. Chung and H.-S. Kim, Photonic Welding of Ultra-Long Copper Nanowire Network for Flexible Transparent Electrodes Using White Flash Light Sintering, *RSC Adv.*, 2016, **6**, 4770–4779.

14 S. Han, S. Hong, J. Yeo, D. Kim, B. Kang, M. Y. Yang and S. H. Ko, Nanorecycling: Monolithic Integration of Copper and Copper Oxide Nanowire Network Electrode through Selective Reversible Photothermochemical Reduction, *Adv. Mater.*, 2015, **27**, 6397–6403.

15 H. Guo, N. Lin, Y. Chen, Z. Wang, Q. Xie, T. Zheng, N. Gao, S. Li, J. Kang, D. Cai, *et al.*, Copper Nanowires as Fully Transparent Conductive Electrodes, *Sci. Rep.*, 2013, **3**, 2323.

16 W. H. Xu, L. Wang, Z. Guo, X. Chen, J. Liu and X. J. Huang, Copper Nanowires as Nanoscale Interconnects: Their Stability, Electrical Transport, and Mechanical Properties, *ACS Nano*, 2015, **9**, 241–250.

17 D. V. Ravi Kumar, K. Woo and J. Moon, Promising Wet Chemical Strategies to Synthesize Cu Nanowires for Emerging Electronic Applications, *Nanoscale*, 2015, **7**, 17195–17210.

18 M. Jin, G. He, H. Zhang, J. Zeng, Z. Xie and Y. Xia, Shape-Controlled Synthesis of Copper Nanocrystals in an Aqueous Solution with Glucose as a Reducing Agent and Hexadecylamine as a Capping Agent, *Angew. Chem., Int. Ed.*, 2011, **50**, 10560–10564.

19 Z. Yin, C. Lee, S. Cho, J. Yoo, Y. Piao and Y. S. Kim, Facile Synthesis of Oxidation-Resistant Copper Nanowires toward Solution-Processable, Flexible, Foldable, and Free-Standing Electrodes, *Small*, 2014, **10**, 5047–5052.

20 M. Mohl, P. Pusztai, A. Kukovecz, Z. Konya, J. Kukkola, K. Kordas, R. Vajtai and P. M. Ajayan, Low-Temperature Large-Scale Synthesis and Electrical Testing of Ultralong Copper Nanowires, *Langmuir*, 2010, **26**, 16496–16502.

21 M. Kevin, G. Y. R. Lim and G. W. Ho, Facile Control of Copper Nanowire Dimensions via the Maillard Reaction: Using Food Chemistry for Fabricating Large-Scale Transparent Flexible Conductors, *Green Chem.*, 2015, **17**, 1120–1126.

22 D. V. R. Kumar, I. Kim, Z. Zhong, K. Kim and D. Lee, Synthesis of Cu Nanowires: Exploring the Dual Role of Alkyl Amines, *Phys. Chem. Chem. Phys.*, 2014, **16**, 22107–22115.

23 Y. Xia, Y. Xiong, B. Lim and S. E. Skrabalak, Shape-Controlled Synthesis of Metal Nanocrystals: Simple Chemistry Meets Complex Physics?, *Angew. Chem., Int. Ed.*, 2009, **48**, 60–103.

24 H. J. Yang, S. Y. He and H. Y. Tuan, Self-Seeded Growth of Five-Fold Twinned Copper Nanowires: Mechanistic Study, Characterization, and SERS Applications, *Langmuir*, 2014, **30**, 602–610.

25 Y. Xiong and Y. Xia, Shape-Controlled Synthesis of Metal Nanostructures: The Case of Palladium, *Adv. Mater.*, 2007, **19**, 3385–3391.

26 D. Zhang, R. Wang, M. Wen, D. Weng, X. Cui, J. Sun, H. Li and Y. Lu, Synthesis of Ultralong Copper Nanowires for High-Performance Transparent Electrodes, *J. Am. Chem. Soc.*, 2012, **134**, 14283–14286.

27 F. Meng and S. Jin, The Solution Growth of Copper Nanowires and Nanotubes Is Driven by Screw Dislocations, *Nano Lett.*, 2012, **12**, 234–239.

28 E. H. Sondheimer, *The Mean Free Path of Electrons in Metals*, 1952, vol. 1.

29 Q. Huang, C. M. Lilley, M. Bode and R. Divan, Surface and Size Effects on the Electrical Properties of Cu Nanowires, *J. Appl. Phys.*, 2008, **104**, 023709.

30 Y.-T. Huang, C.-W. Huang, J.-Y. Chen, Y.-H. Ting, S.-L. Cheng, C.-N. Liao and W.-W. Wu, Mass Transport Phenomena in Copper Nanowires at High Current Density, *Nano Res.*, 2016, **9**, 1071–1078.

31 Q. Huang, C. M. Lilley and R. Divan, An *in Situ* Investigation of Electromigration in Cu Nanowires, *Nanotechnology*, 2009, **20**, 75706.

32 C. Durkan and M. E. Welland, Analysis of Failure Mechanisms in Electrically Stressed Gold Nanowires, *Ultramicroscopy*, 2000, **82**, 125–133.

33 J. Yeo, G. Kim, S. Hong, J. Lee, J. Kwon, H. Lee, H. Park, W. Manoroktul, M. T. Lee, B. J. Lee, *et al.*, Single Nanowire Resistive Nano-Heater for Highly Localized Thermo-Chemical Reactions: Localized Hierarchical Heterojunction Nanowire Growth, *Small*, 2014, **10**, 5015–5022.

34 C. Durkan, M. a. Schneider and M. E. Welland, Analysis of Failure Mechanisms in Electrically Stressed Au Nanowires Analysis of Failure Mechanisms in Electrically Stressed Au Nanowires, *J. Appl. Phys.*, 1999, **1280**, 1280–1286.